

Closed-loop recycling of mixed polyesters via catalytic methanolysis and monomer separations

Received: 7 January 2025

Accepted: 8 August 2025

Published online: 8 September 2025

 Check for updates

Julia B. Curley^{1,2}, Yuanzhe Liang , Jason S. DesVeaux , Hoon Choi , Ryan W. Clarke^{1,2}, Anjani K. Maurya , William E. Michener^{1,2}, Lisa M. Stanley^{1,2}, Yue Wu , Sarah A. Hesse , Andrea L. Baer , Hudson A. Neyer , Christopher J. Tassone^{2,4}, Alan J. Jacobsen⁵, Ofei D. Mante⁵, Gregg T. Beckham & Katrina M. Knauer 

A sustainable plastics future will require high recycling rates and the use of biogenic feedstocks, which together are catalyzing interest in replacing fossil fuel-derived, noncircular polyolefin packaging materials with bio-based, chemically recyclable polyesters. Here we present a catalytic methanolysis process capable of depolymerizing both fossil fuel- and bio-based polyesters, including polyethylene terephthalate (PET), polylactic acid, polybutylene adipate terephthalate and polybutylene succinate in one reactor under mild conditions with high monomer yields. We scaled this process to 1 kg and integrated separations engineering using activated carbon, crystallization, extraction and distillation to remove contaminants and recover individual monomers from depolymerized mixed polyesters with high yield and purity. PET synthesized from monomers isolated from postconsumer materials showed comparable mechanical and thermal properties to PET from commercial monomers. Techno-economic analysis and life cycle assessment show that this process is economically viable and exhibits lower environmental impacts than primary production of respective polymers.

Recent studies have shown that the environmental impacts of the plastics industry could be reduced substantially by increasing the use of bio-based materials, boosting recycling rates and integrating carbon capture technologies^{1–6}. To this end, bio-based polyesters offer a promising solution due to their sourcing from biogenic feedstocks, tunable properties and potential for selective chemical and biological degradation^{7–11}. To meet the circular economy goals of the plastics industry, energy-efficient recycling methods for these materials are urgently needed, especially as the market for bio-based polyesters continues to grow^{12–14}.

Fully or partially bio-based polyesters, such as polylactic acid (PLA), polybutylene adipate terephthalate (PBAT) and polybutylene succinate (PBS), can be selectively depolymerized to monomers through cleavage of the common ester bond via well-known methods^{15–17}. These polyesters are used in diverse applications including compostable packaging and cutlery, agricultural film and 3D printing filament. Furthermore, these products often comprise multiple polyesters to achieve suitable material properties and biodegradation behavior (for example, agricultural film is often a blend of PLA, PBAT and starch-based compounds).

¹Renewable Resources and Enabling Sciences Center, National Renewable Energy Laboratory, Golden, CO, USA. ²Bio-Optimized Technologies to keep Thermoplastics out of Landfills and the Environment (BOTTLE) Consortium, National Renewable Energy Laboratory, Golden, CO, USA. ³Catalytic Carbon Transformation and Scale-Up Center, National Renewable Energy Laboratory, Golden, CO, USA. ⁴Stanford Synchrotron Radiation Lightsource, SLAC National Accelerator Laboratory, Menlo Park, CA, USA. ⁵Amazon Corporation, Seattle, WA, USA.  e-mail: katrina.knauer@nrel.gov

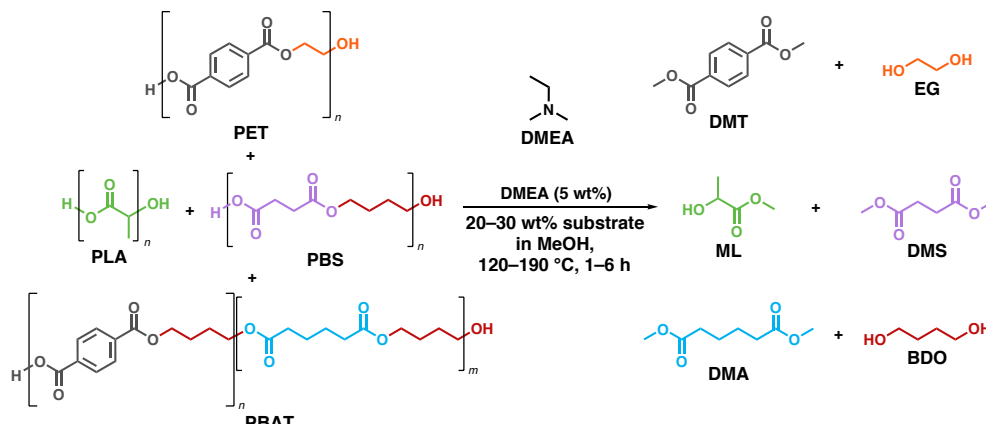


Fig. 1 | Polymer backbone structures of polyester waste feedstocks, methanolysis conditions studied and deconstructed monomeric products.

Despite this, mixed polyester chemical recycling on real-world substrates remains relatively underexplored^{18–20}. Mechanical recycling, the predominant recycling method at scale, cannot meet this need because it requires a high-purity, single-polymer input¹⁷. Similarly, ongoing commercial chemical recycling efforts for polyesters are focused on single feedstocks, primarily petroleum-based polyethylene terephthalate (PET)^{17,21}. To address the complexity of mixed, postconsumer feedstocks containing diverse impurities, a versatile chemical recycling approach that complements mechanical recycling is essential²². Postconsumer waste materials contain a wide variety of additives and impurities; thus, depolymerization and downstream separation processes must be able to tolerate low-purity feedstocks and generate high-purity monomers as drop-in replacements for polyester repolymerization^{17,23–26}. Finally, integration of techno-economic analysis (TEA) and life cycle assessment (LCA) is crucial to guide the development of these processes, both to balance cost-effectiveness with environmental sustainability and to identify primary process drivers^{27,28}.

Our recent TEA–LCA modeling study compared multiple processes for polyester degradation and identified amine-catalyzed methanolysis (ACM) as the most cost-effective and environmentally beneficial method for recycling a mixed feedstock of PET, PLA and PBAT under the studied conditions²⁹. PET was included in the selected feedstock for this study because it is produced in large volumes, is widely collected through curbside recycling programs and serves as a representative material to demonstrate that both fossil-based and bio-based polyesters can be recycled together in a commingled stream—reducing the burden on waste sorting systems. A key feature of ACM is the volatile amine catalyst, dimethylethylamine (DMEA), which can be recovered from the reaction mixture by distillation after depolymerization. In addition, the methyl ester monomers resulting from ACM are easier to separate and purify via conventional unit operations than the acid (from hydrolysis) or 2-hydroxyethyl ester (from glycolysis) analogs. The ACM-derived monomer products can be directly repolymerized to the parent polymers via transesterification, enabling closed-loop recycling of both petroleum and bio-based polyesters^{30–32}. Our previous modeling study also outlined key areas for improving monomer yields, recovery efficiency and energy intensity, although experimental validation and expansion of the feedstocks to other commercial bio-based polyesters, such as PBS, were not yet conducted. The application of TEA and LCA enabled a priori selection of an optimal chemical recycling strategy for mixed polyester streams before experimental efforts were initiated.

Here we present experimental evaluation and optimization of an ACM process for mixed polyester recycling with integrated monomer separations and repolymerization (Extended Data Fig. 1). We first optimized the depolymerization conditions for PET, PLA, PBAT and PBS at gram scale, then demonstrated the ACM process on 1 kg of mixed model

PET feedstock. *In situ* X-ray scattering experiments provided insight into depolymerization reaction kinetics and polymer morphology. Based on our process modeling efforts, we validated a downstream separation process to achieve effective contaminant removal and high-purity monomers. This entailed dimethyl terephthalate (DMT) recovery via crystallization and distillation, contamination removal via activated carbon (AC) and ion-exchange (IX) treatment, methyl lactate (ML) recovery via distillation, separation of diols and diesters via liquid–liquid extraction (LLE), and recovery of individual diols and diesters via distillation. With the exception of the diol and diester distillations (which are well established and were modeled in Aspen), all separation steps were validated experimentally. To demonstrate the purity of the recovered monomers, PET was repolymerized using DMT recovered and purified from postconsumer waste substrates. Comprehensive process modeling, TEA and LCA were refined and validated by the experimental results to demonstrate that, at scale, this process is estimated to be cost-competitive with virgin polyester plastics while reducing the greenhouse gas (GHG) emissions and other environmental impacts of polyester production.

Results

Gram-scale deconstruction optimization

All polymer substrates used in this study were fully characterized according to Cuthbertson et al.³³, with results presented in Supplementary Information section I (Supplementary Figs. 1–24 and Supplementary Table 1). Initial deconstruction reactions were conducted at a 10-mL scale using PET, PLA, PBAT or PBS at 20 wt% polymer loading in methanol (MeOH) with 5 wt% DMEA catalyst loading relative to polymer (Fig. 1; see Methods and Supplementary Fig. 25). Reactions were conducted at temperatures ranging from 120 °C to 190 °C for 2 h to investigate trends in polymer reactivity, with monomer yields determined by gas chromatography–mass spectrometry (GC–MS) (Fig. 2a). These experiments indicated that PLA is the most reactive polymer in this system, with ML yields >80% achieved even at 120 °C. Conversely, high DMT yields from PET were not observed until reaction temperatures reached 170 °C. DMT from PBAT was obtained in higher yields than DMT from PET under most conditions tested, potentially due to differences in polymer solubility at reaction temperatures (vide infra) or accessibility of the polymer to the catalyst due to aliphatic components. Dimethyl adipate (DMA) from PBAT and dimethyl succinate (DMS) from PBS followed a similar trend in yields, and all polymers studied reached 80–90% monomer yields after 2 h at 170 °C. Because deconstruction of polycondensation polymers is typically equilibrium-limited, these results are approaching the maximum possible yields, particularly when accounting for inevitable losses during quantification by GC–MS³⁴.

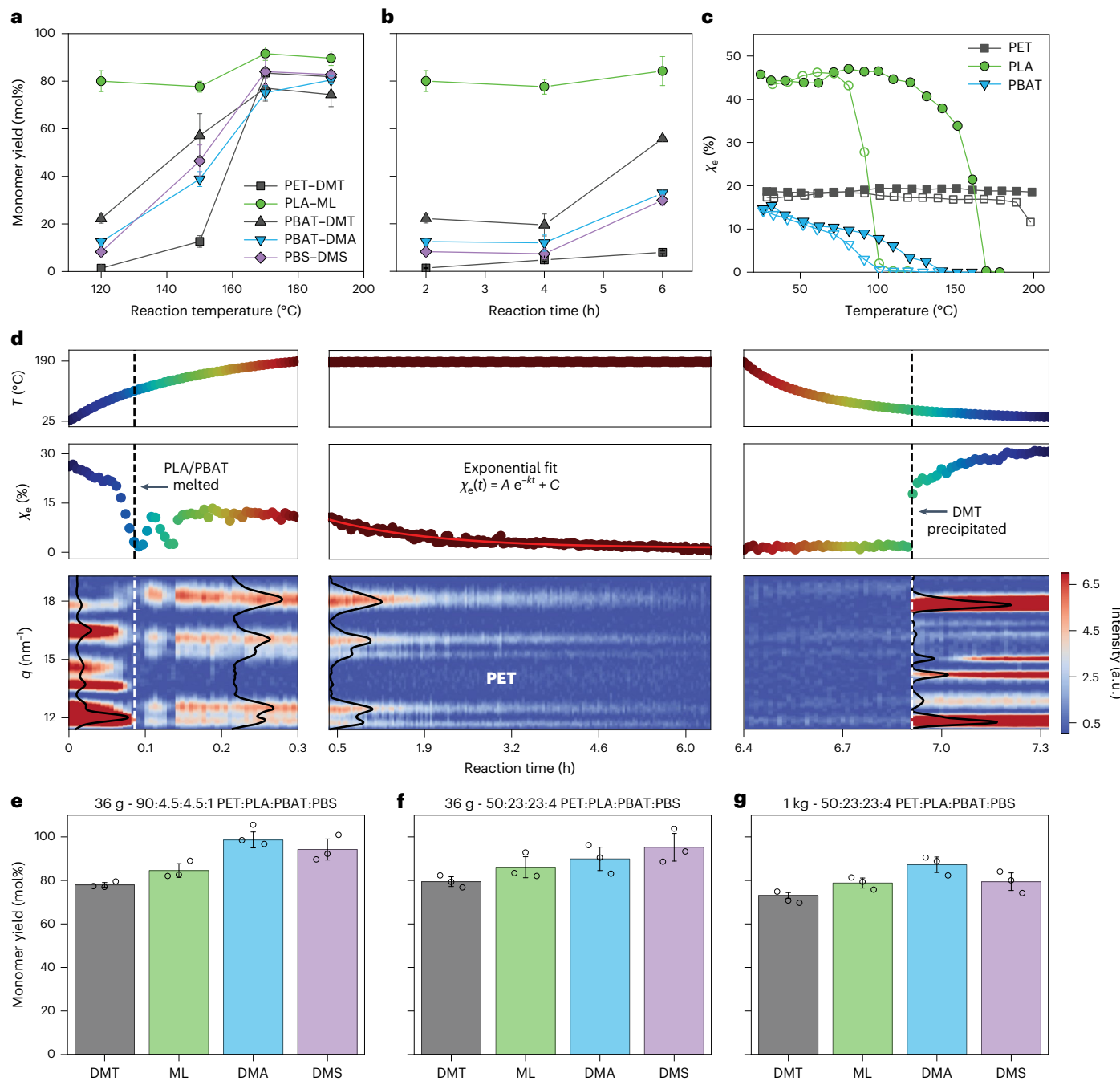


Fig. 2 | Polyester deconstruction and polymer behavior from in situ WAXS.

a, Yields of monomers from PET, PLA, PBAT and PBS in single-polymer depolymerization reactions at 120, 150, 170 and 190 °C for 2 h. **b**, Yields of monomers from PET, PLA, PBAT and PBS in single-polymer depolymerization reactions at 120 °C for 2, 4 and 6 h. **c**, The effect of MeOH on the estimated degree of crystallinity (χ_e) for PET, PLA and PBAT as a function of temperature, demonstrating depression in melting point of polymers in the presence of MeOH. Filled symbols indicate the behavior of polymer alone; empty symbols indicate the behavior of polymer in MeOH. Formula and calculation for χ_e described in Supplementary Information section XVI. **d**, In situ WAXS measurement illustrating the deconstruction reaction of a mixture comprising PET, PLA and PBAT (50:25:25) in MeOH with DMEA, alongside the estimated degree of crystallinity (χ_e) and the WAXS profiles plotted against reaction time and temperature. Here, q is the magnitude

of the scattering vector with intensity graphed as a heat map; formula and calculation described in Supplementary Information section XVI. **e**, Yields of DMT, ML, DMA and DMS from 36 g mixed feedstock at 90:4.5:4.5:1 PET:PLA:PBAT:PBS. **f**, Yields of DMT, ML, DMA and DMS from 36 g mixed feedstock at 50:23:23:4 PET:PLA:PBAT:PBS, showing the tolerance of this methanolysis system to a variable mixed polyester feedstock. **g**, Yields of DMT, ML, DMA and DMS from 1 kg mixed feedstock at 50:23:23:4 PET:PLA:PBAT:PBS, demonstrating the scalability of this process. Reaction conditions for **a** and **b**: 2 g polymer(s), 8.00 g MeOH (10.1 ml), 0.100 g DMEA (143 µl) at designated reaction temperature and time. Reaction conditions for **e** and **f**: 36 g polymers, 143 g MeOH (182 ml), 3.60 g DMEA (5.16 ml) at 190 °C for 3 h. Reaction conditions for **g**: 1 kg polymers, 3.80 kg MeOH (4.80 L), 100 g DMEA (143 ml) at 190 °C for 3 h. Error bars shown are the standard deviations obtained from triplicate trials with values centered on the mean.

Due to the stark difference in polymer reactivity at 120 °C, we next investigated longer depolymerization times at this temperature to further elucidate differences in ACM reactivity (Fig. 2b). No changes in monomer yields outside of triplicate error bars were observed between

2-h and 4-h reaction times, but at the 6-h reaction time, all polymers except PET reached >25% conversion to monomers. This indicates an induction period in the depolymerization of PBAT and PBS at 120 °C and further highlights that PET is the most recalcitrant feedstock polymer.

We next transitioned from single-polymer experiments to a mixed-polymer system to deconstruct all four polyesters in one reaction. To optimize the reaction conditions, we used a lean six-sigma design of experiments (DOE) approach (details and data in Supplementary Information section III, Supplementary Figs. 26–36 and Supplementary Tables 2 and 3). The influence of four factors was studied in triplicate reactions: 50–90 wt% PET (PLA:PBAT:PBS mass ratio of 5:5:1 held constant), 20–30 wt% total solids loading, 150–190 °C reaction temperature and 1–5 h reaction time. The PET loading variable was used to ensure high monomer yields with changing mixed polyester feedstock, as is predicted in real polyester markets²². The yields of DMT, ML, DMA and DMS were measured as response factors, in addition to a weighted yield metric defined as the mol% yield of each monomer multiplied by the percent loading of its parent polymer(s) to indicate the overall success of a reaction. Temperature and time exhibited the greatest impact on all response factors, while PET loading and total solids loading did not have a statistically significant impact on all monomer yields according to the Pareto chart (Supplementary Table 3). A solids loading of 20 wt% was chosen in our final optimized conditions to improve processability and slightly increase yields. TEA performed on the process (*vide infra*) revealed that reaction time had a greater impact on process costs than reaction temperature (Supplementary Fig. 37), although the impacts of both were relatively minor. Therefore, 190 °C and 3 h were selected as the optimized mixed polyester depolymerization conditions. A variety of postconsumer substrates were deconstructed under the optimized conditions to demonstrate the applicability of this system to real waste streams (Supplementary Information section IV and Supplementary Fig. 38).

In situ X-ray scattering insights into ACM

To better understand the behavior of mixed PET, PLA and PBAT during depolymerization, we conducted wide-angle X-ray scattering (WAXS) measurements to explore the impact of solvent on polymer structure across different temperatures (Supplementary Figs. 39–41). PBS was not included in these studies owing to its current low production volumes and to avoid overcomplicating the scattering profiles. In the presence of methanol, PBAT melted at -100 °C, PLA at -110 °C, and PET initiated melting at -180 °C (Fig. 2c). This corresponds to a melting point depression compared with neat polymer of -40, -60 and -80 °C, respectively³⁵. Notably, PET was the only polymer that did not completely melt at the reaction temperature of 190 °C. This melting point depression is due to strong interactions between the ester groups and the methanol, which reduce the chemical potential of the molten phase of the polymer. According to Flory–Huggins theory, this chemical potential reduction lowers the equilibrium melting point of these polymers^{36,37}. The existence of PLA and PBAT in a predominantly molten state across batch reaction conditions could explain the higher deconstruction yield observed for these polymers compared with PET, which remains incompletely melted during the deconstruction process and therefore limits access of the solvent and catalyst to the surface of polymer crystalline domains³⁸.

We performed *in situ* WAXS measurements to investigate the deconstruction of mixed PET, PLA and PBAT in ACM (Methods). The WAXS profiles and estimated degree of crystallinity are plotted as a function of temperature and time in Fig. 2d. While ramping the temperature from 25 to 190 °C, PLA and PBAT melted around 100–110 °C, similar to the melting point depression observed in the presence of methanol. At 190 °C, PET diffraction peaks were still observed, indicating incomplete melting. Holding the reaction temperature at 190 °C led to a gradual decrease in the intensity of PET diffraction peaks and a reduction in the estimated degree of crystallinity. We obtained a rate of crystalline fraction loss at 190 °C of 5% per hour. The intensity of PET diffraction peaks at 190 °C significantly decreased after 2–3 h, which aligns with the chosen optimized batch-reaction conditions. One of the rate-limiting factors for the deconstruction of PET could be the

breakdown of crystallites from the particle surface, as solvents and catalysts do not penetrate into the crystalline domains of polymers^{38,39}. Upon cooling, we observed strong diffraction peaks corresponding to DMT crystals, which precipitated at -55 °C. No significant peaks were observed from PET, PLA and PBAT, confirming the breakdown of these polymers into their respective monomers. Taken together, these X-ray scattering results indicate that polymer melting may accelerate polymer deconstruction and that our chosen deconstruction conditions effectively breakdown the feedstock polymers.

Deconstruction reactions up to the 1 kg scale

We next scaled mixed polyester methanolysis from a substrate mass of 2 g to 36 g using a 300-ml pressure reactor (Methods) and a 90:4.5:4.5:1 PET:PLA:PBAT:PBS ratio to approximately represent current PLA, PBAT, and PBS production volume ratios²² (Fig. 2e). All monomer yields were 78–98% under the optimized conditions. Next, the feedstock composition was changed to 50:23:23:4 PET:PLA:PBAT:PBS to represent possible future production volume ratios (Fig. 2f). A decrease in DMA yield of 8% to 90% was observed, just outside the standard deviation from triplicate experiments, while all other monomer yields were within error (95% confidence interval, CI), demonstrating the tolerance of this depolymerization process to a highly variable feedstock. Finally, the reaction was scaled to 1 kg 50:23:23:4 PET:PLA:PBAT:PBS in a 7.7-liter pressure reactor (Methods). The DMS yield decreased by 15% but remained high at 79%, while the remainder of the monomer yields were within error of the 36 g scale (95%CI) reactions at the same feedstock ratio (Fig. 2g). These experiments demonstrate the feasibility of this process to depolymerize a mixed and variable feedstock of PET, PLA, PBAT and PBS.

Process development for monomer separations

Due to the heterogeneity of mixed postconsumer plastic waste and the need for highly pure monomers for successful condensation polymerization, rigorous separations processes are required to achieve effective contaminant removal and reclaim pure monomers. Accordingly, a separation sequence was designed consisting of DMT recovery via crystallization and distillation, contamination removal via AC and IX treatment, ML recovery via distillation, separation of diols (1,4-butanediol (BDO) and ethylene glycol (EG)) and diesters (DMA and DMS) via LLE, and recovery of individual diols and diesters via distillation (Fig. 3a; see detailed discussion below). The yields and purities for DMT distillation and crystallization, AC treatment and LLE were determined experimentally from mixed postconsumer waste feedstocks, while those for distillation of monomers were determined in Aspen Plus (Fig. 3b and Supplementary Table 4). A detailed outline of the monomer recovery/purification steps with associated purities and photographs is shown in Extended Data Fig. 2 and Supplementary Fig. 42.

Experimental purification of DMT from postconsumer waste

An ACM reaction was run using 36 g mixed postconsumer materials, including postconsumer recycled PET bottle flake, compatibilized PLA/PBAT compost bags and PBS/cellulose candy packaging^{40,41} (details in Supplementary Information section VIII, Supplementary Tables 5–7 and Supplementary Figs. 43–45). Monomer yields from this experiment were 83% for DMT, 87% for ML, 83% for DMA and 82% for DMS. Crude DMT, along with polyolefins and other contaminants, were isolated via filtration (Supplementary Information section IX and Supplementary Figs. 46–48). The DMT was further purified via distillation at 150 °C and 2 Torr, followed by recrystallization from 80 °C MeOH, yielding 72.7% overall recovery from the crude product and a purity of 99.4% (Supplementary Fig. 44). DMT recovery data were used to refine the process model, and the purified monomer was used to repolymerize to PET (*vide infra*).

Experimental AC treatment of ACM liquid mixtures

Inductively coupled plasma mass spectrometry (ICP-MS) performed on the post-ACM liquid mixture confirmed the presence of ten metals

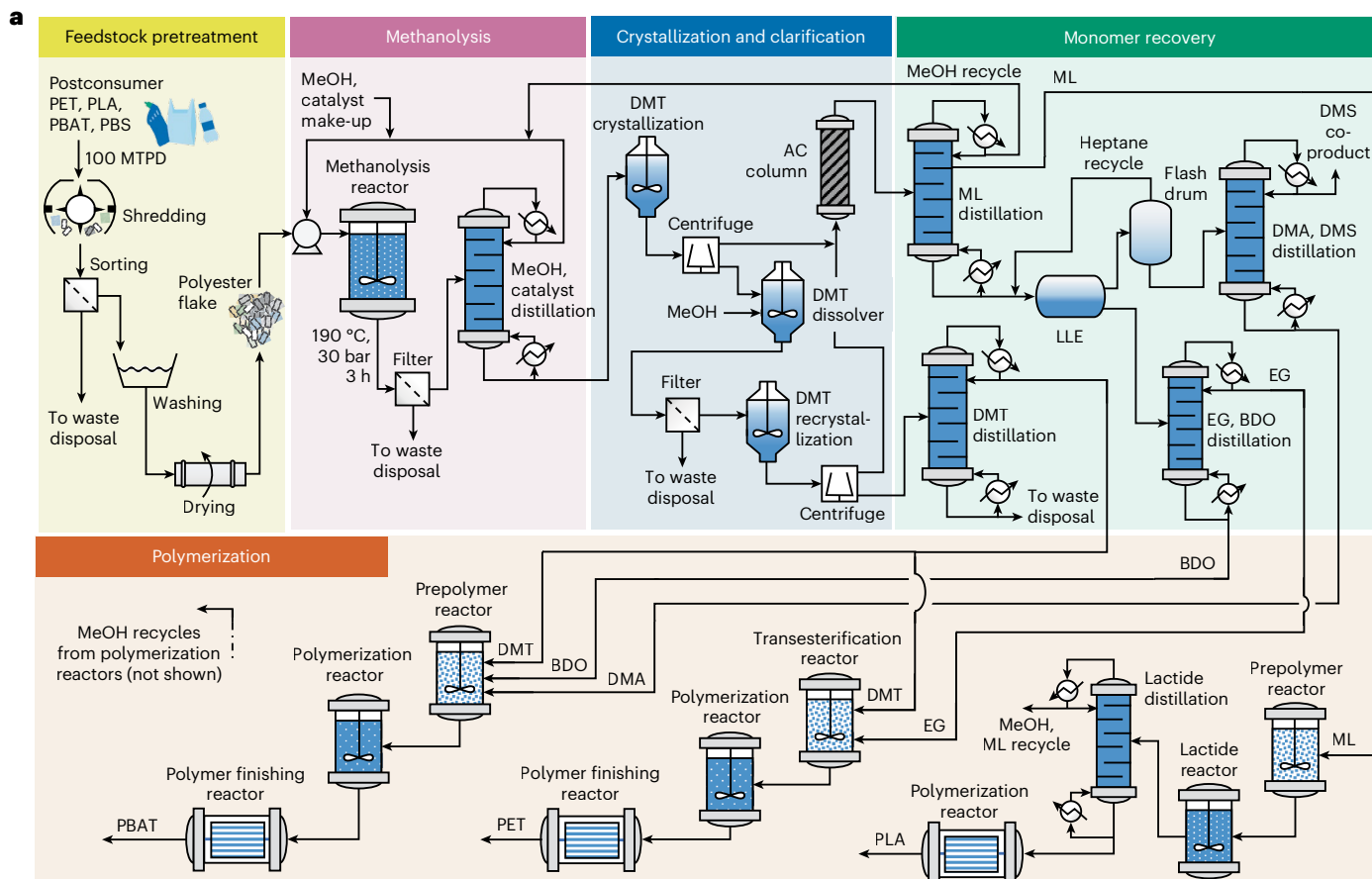


Fig. 3 | Process flow diagram and modeled and experimental downstream processing. **a**, Simplified process flow diagram for ACM of PET, PLA, PBAT and PBS delineated by process area. Detailed process flow diagrams for all sections of the process are shown in Supplementary Figs. 51–60. **b**, Normalized monomer yields, using combined experimental and modeled data, through the downstream separation process for a 50:23:23:4 PET:PLA:PBAT:PBS feedstock. **c**, Dye and metals removal via AC treatment of postcrystallization, soluble monomer fractions. ‘Original feed’ denotes the metal composition

breakdown in the liquid monomer mixture after depolymerization and filtration, ‘breakthrough’ denotes the mass center of a breakthrough curve and ‘plateau’ denotes a saturation point after the breakthrough curve reaches a plateau (Supplementary Fig. 49a). **d**, Average recovery yield of DMA and DMS from diols via LLE with heptane. The monomer mixture contains BDO, EG, DMA and DMS in a volume ratio of 1:1:1 and the solvent-to-mixture volume ratio was 1:1 for one-step and 0.5:1 for two-step LLE. Error bars shown are the standard deviations obtained from triplicate trials centered on the mean.

in quantities greater than 4 ppm, with particularly high Sb levels (21.4 ppm), presumably due to its use as a catalyst in PET polymerization⁴² (Fig. 3c, left, Supplementary Fig. 49 and Supplementary Table 8). After DMT removal, the liquid fraction was run through a packed AC column (0.27 g AC per milliliter bed volume) to determine the efficacy of AC for removing colorant and metal contaminants. In a breakthrough curve, the effluent was colorless until the bed was saturated, indicating the effective removal of colorants (Fig. 3c, inset

photos). Accordingly, a dynamic loading capacity was determined as 17 ml g⁻¹ AC before the effluent changes from colorless back to green, which is similar to previous literature AC treatment studies^{43,44}. The ICP-MS results show that the AC treatment also reduced the concentration of all metals below 1 ppm apart from Sb, which decreased to 2.3 ppm (Fig. 3c, middle). The column can be regenerated with steam or methanol, which can be recycled back into the ACM process^{45,46}.

Experimental diol and diester separation via LLE

To avoid distillation, LLE was used to separate the diols from the methyl ester monomers. We found that addition of pentane, hexane, heptane or water was sufficient to achieve effective phase separation between the diol and methyl ester monomers owing to their polarity difference (Fig. 3d and Supplementary Fig. 50). Adding water was less favorable for this process owing to its higher heat of vaporization compared with volatile hydrocarbons, so we selected heptane as the LLE solvent due to its low cost and safer handling than other volatile alkanes.

Both increasing the volume ratio of hydrocarbon solvent to monomer mixture and increasing the number of LLE steps enhanced separation efficiency (Supplementary Information section XI). For instance, the recovery yield for the diesters increased from 99.2% to 99.6% by varying the solvent-to-monomer mixture volume ratio from 1:1 to 16:1. At a 1:1 solvent-to-mixture ratio, increasing from one-step to two-step LLE improved the recovery yield from 99.6% to 99.8% (Fig. 3d and Supplementary Tables 9 and 10). TEA indicated that minimizing the solvent-to-mixture volume ratio was most important for reducing the energy requirements of heptane distillation, while increasing the volume ratio resulted in minimal increases to the separation efficiency; thus, a three-step LLE at 1:1 volume ratio was selected for the process model.

Monomer yields through downstream processing

The process model was refined and improved using experimental data from the methanolysis reaction, DMT crystallization, AC treatment and LLE. Modeled monomer yields as the reaction products travel through the separation process train are shown in Fig. 3b. Polymer and monomer losses occur throughout the process and are sent to solid, organic and wastewater treatment. The first product recovered, DMT, exhibited a 75% overall monomer yield after 2% and 4% losses in crystallization and distillation, respectively. The AC and IX treatments led to a yield loss of 1–2% of EG and BDO monomers and 5–6% monomer yield loss for ML, DMA and DMS monomers attributed to higher adsorption to the AC. The final recovery yield of ML was 78% after a 5% yield loss during distillation. The subsequent LLE step resulted in 1–5% monomer yield losses. Lastly, the distillation separations resulted in yield losses of less than 1% for DMA, EG and BDO and a loss of 3% DMS due to its low concentration; the overall yields after distillation were 72% for EG, 81% for BDO, 81% for DMA and 72% for DMS. To demonstrate the circularity of our chemical recycling technology, we next synthesized PET using DMT obtained through methanolysis of postconsumer materials as described above. The purified DMT was polymerized with commercial EG in a polycondensation reactor to obtain recycled PET (Fig. 4a and Methods), whose thermal and mechanical properties were compared with PET synthesized from commercial DMT purified via distillation and crystallization (Supplementary Figs. 61 and 62). Gel permeation chromatography (GPC; Fig. 4b), tensile testing (Fig. 4c), and differential scanning calorimetry (DSC) (Fig. 4d) show minimal differences in molar mass, molar mass distribution, elongation at break, tensile strength and thermal properties between the polymers. The recycled PET retained a pristine white color and the resulting DSC (Fig. 4d) and thermogravimetric analysis curves (Supplementary Fig. 61) showed a highly pure polymer. This experiment indicates that PET can be recycled in this process with no deterioration in properties. The synthesis of polymerization-purity lactide from ML obtained from the deconstruction of postconsumer PLA waste was also demonstrated, with a measured purity of 99.0% (Supplementary Information section XIV and Supplementary Figs. 63–68).

Process modeling and economic analysis

To evaluate the performance of the mixed polyester ACM process at scale, we updated our previously developed process model²⁹ based on experimental findings. The proposed process is shown in Fig. 3a and briefly described here with detailed descriptions, diagrams and stream tables provided in Supplementary Information section XII. The

base-case plant was modeled to have a capacity of 100 metric tons per day (MTPD). The mixed polyester bale feedstock was assumed to have a purity of 90 wt% and be purchased at a cost of US\$0.30 kg⁻¹ based on postconsumer PET thermoform bales due to a lack of data for the envisioned feedstock. The process begins with feedstock pretreatment, which involves flaking, float–sink sortation, washing and drying. The polyester flake is then mixed with DMEA at 5 wt% (relative to the polyester feedstock content) and MeOH to create a 20 wt% slurry. The slurry is pumped to a continuously stirred methanolysis reactor operating at 190 °C and 30 bar with a residence time of 3 h where 90% PET, 85% PLA, 90% PBAT and 85% PBS are converted to monomer products. The reaction solution is filtered to remove insoluble contaminants, and the filtrate is cooled to precipitate polyolefins (Supplementary Information section IX), then distilled to recycle DMEA and MeOH, resulting in a concentrated stream of soluble monomer products.

DMT is crystallized from solution, and the mother liquor is pumped through ultrafiltration to remove residual solids and then passed through AC and IX columns where colorants and contaminants are removed. The DMT is recrystallized in MeOH, distilled and sent to polymerization. The clarified monomer solution is distilled to remove ML, MeOH and residual DMEA in the distillate, leaving the methyl ester and diol products in the bottoms stream. The distillate is then sent to a second distillation column to purify ML, which is sent to polymerization, and recycled MeOH and DMEA to the depolymerization reactor. The methyl ester and diol solution undergoes a three-stage counter-current LLE with heptane. The diol fraction is distilled to separate EG and BDO, which are sent to polymerization; the heptane fraction is distilled to recover and recycle heptane, and the methyl esters are further distilled to recover DMS, which is sold as a co-product due to its low volume, and DMA, which is sent to polymerization. The recovered monomers are then polymerized to their respective polymers: ML is reacted to form lactide, which is distilled then sent to ring opening polymerization³⁰; DMT and EG are transesterified then undergo polycondensation to PET; DMT, DMA and BDO are reacted to an intermediate then undergo polycondensation to PBAT^{47,48}. With DMT being used in both PET and PBAT polymerization, the split was set on the basis of the DMA flow rate to PBAT polymerization with the residual quantity sent to PET owing to PBAT's higher market value.

Based on the mass and energy balances from the process model, the capital and operating expenses for the plant were estimated, and a discount cash flow analysis was conducted to determine the minimum selling price (MSP, that is, the average selling price of the PET, PLA and PBAT products for which the total lifetime value of the plant (net present value) is equal to 0; see Supplementary Table 11 for parameters). For the base-case process (Supplementary Table 12), the total direct installed equipment cost (Fig. 5a and Supplementary Table 13) was estimated to be US\$55 million (MM) with the highest contributions from the polymerization and product recovery sections (22% and 21%, respectively) due to the large number of unit operations including distillation columns, reactors and heat exchangers. The remaining process areas exhibited moderate contributions accounting for 9–19% of direct equipment costs. When combined with other direct costs and indirect costs, the estimated total capital investment for the plant is US\$108.5 MM.

Alongside the capital costs, the total operating expense for the plant (Fig. 5b and Supplementary Table 14) was estimated to be US\$33 MM per year, resulting in an MSP of US\$2.37 kg⁻¹ of combined polymeric product (Fig. 5c and Supplementary Table 15). The largest contributor to the MSP at 32% was the capital cost for the process. Feedstock and waste treatment costs each contributed 19% to the MSP. Fixed costs (for example, labor, overhead and maintenance) and raw materials (for example, MeOH, AC replacement and process water) were found to be moderate contributors, accounting for 16% and 8% of the MSP, respectively. Smaller contributions (1–3%) resulted from steam, electricity and other miscellaneous process costs. Due to the small amounts

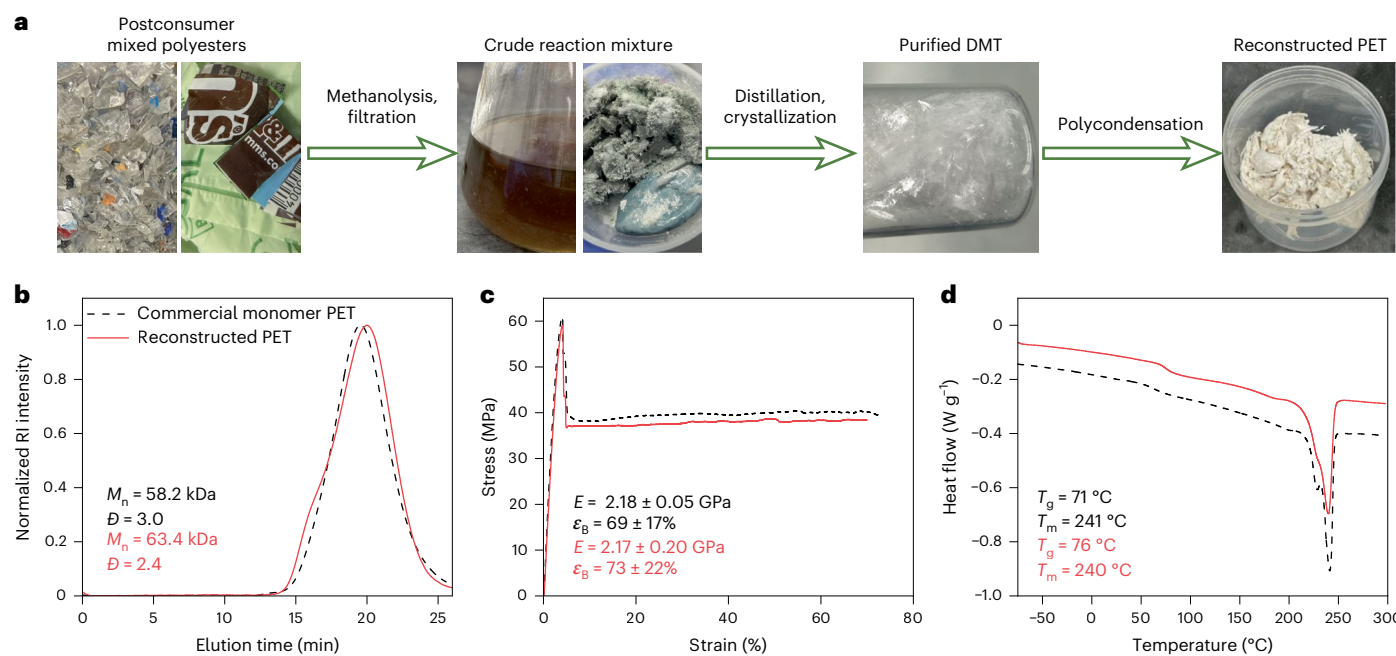


Fig. 4 | Reconstruction of PET from postconsumer materials. **a**, Pictures of the postconsumer mixed polyester substrates, crude reaction mixture, purified DMT and reconstructed PET. **b–d**, GPC based on a refractive index detector (**b**), tensile testing (**c**) and DSC (**d**) of PET synthesized from commercial

monomers compared with reconstructed PET, along with key metrics of each characterization. M_n , number average molar mass; D , dispersity; E , tensile strength; ε_B , elongation at break; T_g , glass transition temperature; T_m , melting temperature.

of PBS in the feedstock (4 wt% in the base case), the resulting DMS was sold as a co-product resulting in a 3% credit to the MSP.

LCA and environmental justice assessment

The impacts from raw material extraction to the factory gate (cradle-to-gate) were evaluated to estimate the environmental impacts for the process. The base case was found to have lower impacts across 11 out of 14 impact categories, including climate change, fossil fuel depletion and water depletion, compared with the virgin production of an equivalent PET, PLA and PBAT product mix (Fig. 5d and Supplementary Table 16). The process showed a 1.7–9.7 times higher impact for human toxicity, freshwater eutrophication and marine eutrophication categories, largely due to high quantities of wastewater generated (1.02 kg kg⁻¹ product) during feedstock pretreatment and IX regeneration. For climate change impact, the ACM process exhibits a 41% reduction in GHG emissions compared with virgin production with process steam use and waste treatment contributing 46% and 25% of the total emissions, respectively (Fig. 5e and Supplementary Table 16). Depolymerization and product recovery accounted for most of the steam consumption due to distillation for solvent recovery and product purifications (Fig. 5f and Supplementary Table 17).

A preliminary environmental risk assessment was performed using the five-part inquiry-based framework outlined in Uekert et al.⁴⁹ to identify process materials with human health or ecological issues related to their production, use or emission for the base-case process. The use of methanol was found to present a key hazard due to its toxicity and flammability. The high temperatures and pressures used in the process would require adherence to known safety standards⁵⁰ to ensure that fugitive emissions and exposure events for workers and local communities are limited. Specific measures to reduce these hazards include automatic pumping systems from chemical storage, adequate ventilation and air detection systems. In addition, the process generates 1.02 kg wastewater and 0.27 kg organic waste kg⁻¹ product in the base case, which is considered hazardous due to methanol concentrations >1 wt% (ref. 51). While the quantities of waste generated are due in part to assumed process losses, the quantities and losses could be decreased

through more intensive distillation before waste treatment. No social or child labor issues were identified. Complete details and results for the materials screened are provided in Supplementary Table 18.

Sensitivity analysis

Key process variables were analyzed through univariate sensitivity analysis to understand their impact on process economics (Fig. 5g and Supplementary Table 19) and climate change (Fig. 5h and Supplementary Table 20). Feedstock cost was found to result in the greatest increase (47%) in MSP at the upper bound US\$1.00 kg⁻¹, representative of a premium price, due to its high contribution to the overall MSP. Similarly, the fixed capital investment and plant size were shown to be highly sensitive variables due to the high capital recovery charge contribution. Depolymerization extent, feedstock purity and solids loading were shown to have high impact on the MSP and GHG emissions due to increased yield losses, waste treatment and steam requirements. When considering the potential for decarbonization of process utilities, renewable electricity decreased the GHG emissions by 4% while process steam and fired heat from renewable natural gas (RNG) showed a substantial 44% decrease.

Discussion

The results presented here suggest that ACM could be an effective method of recycling mixed polyester waste. Future work to determine the industrial feasibility of this process will include determining the kinetics of continuous, mixed polyester deconstruction in reactors similar to the continuous stirred tank reactor modeled here (Fig. 3a). Deconstruction data across conditions also highlight that a sequential reaction approach could be used where polymers such as PLA are solubilized and/or deconstructed first, leading to more facile monomer separations. In addition, the impact of parameters such as the polyester feedstock flake size on deconstruction kinetics should be determined, particularly given the in situ WAXS data, which show that not all polymer substrates enter solution at the reaction temperature (Fig. 2d).

New bio-based polyesters continue to enter the market as demand for sustainable plastics grows. Polyhydroxyalkanoates are one such example that describe a class of materials with varying structural

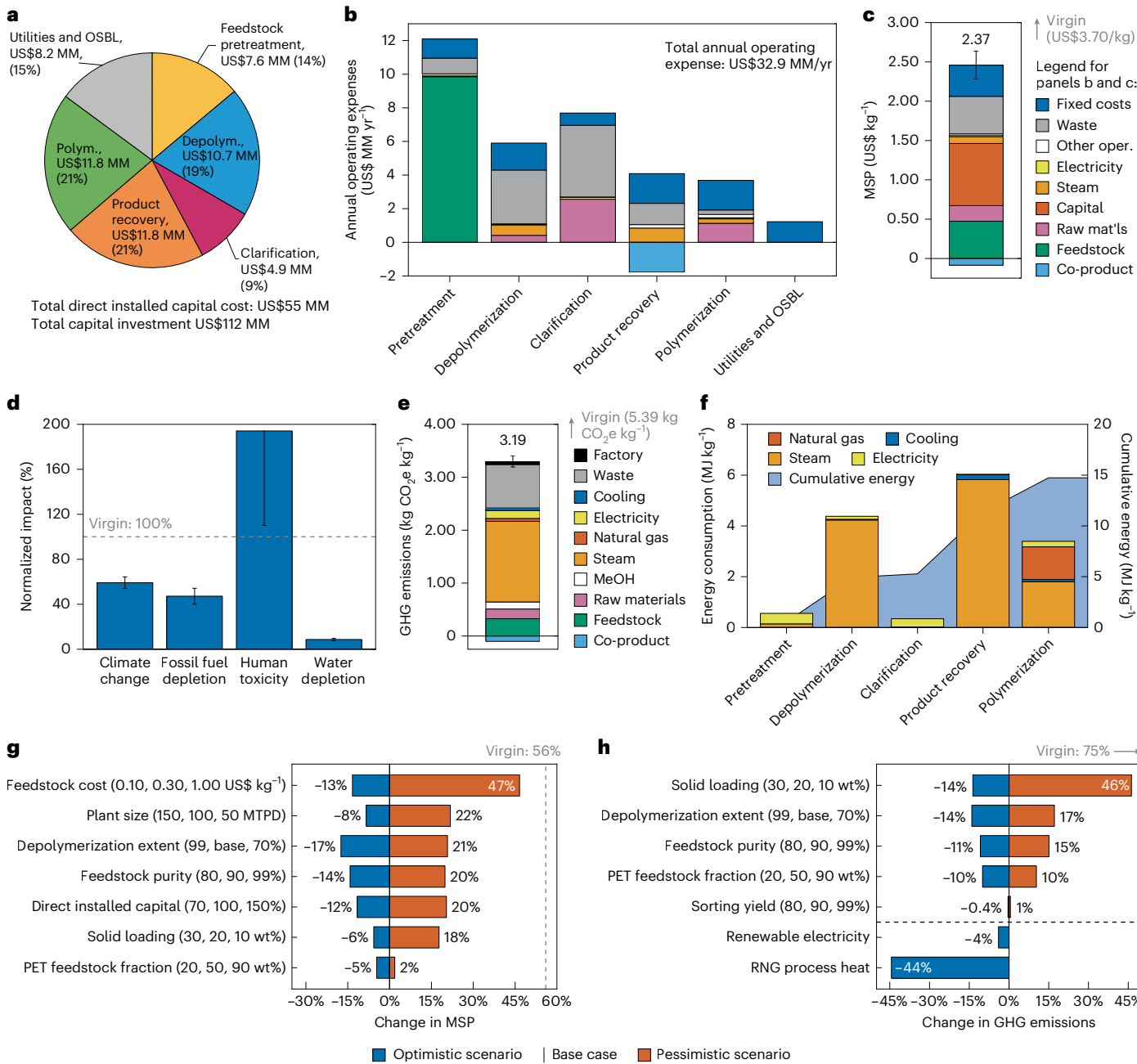


Fig. 5 | Economic and environmental impacts of ACM. All costs shown are for a 2022 USD basis. **a**, Direct installed capital for the 100 MTPD plant in millions of dollars (US\$MM) broken down by process area including utilities and outside battery limits (OSBL) costs. **b**, Annual operating expenses in US\$MM per year divided into component contributions and broken down by process area. The legend is provided to the right of **c**. **c**, MSP for the process broken down by component contribution. The virgin price of US\$3.70 kg⁻¹ for an equivalent mixture of polyesters is shown for reference. Error bar represents the standard deviation determined from Monte Carlo analysis using 1,000 runs centered on the mean. **d**, Cradle-to-gate LCA results for selected impact categories for the methanolysis process normalized to virgin production (shown for reference as a dashed gray line). Error bars represent the standard deviation determined from Monte Carlo analysis using 1,000 runs centered on the mean. **e**, GHG emissions for the process broken down by component contribution. The virgin

GHG emissions of 5.39 kg CO₂ equivalents (CO₂e) per kilogram for an equivalent mixture of polyesters is shown for reference. Error bar represents the standard deviation determined from Monte Carlo analysis using 1,000 runs centered on the mean. **f**, The energy consumption in MJ kg⁻¹ divided into component contributions and broken down into process area. The cumulative energy demand for the process is shown in the background. **g**, **h**, Univariate sensitivity results for the MSP (**g**), and the process GHG emissions with virgin performance (**h**) are shown for reference. Renewable electricity uses the Regional Energy Deployment System mid-case scenario with 95% decarbonization⁵⁴ and renewable natural gas (RNG) process heat uses RNG for fired heat and steam production. The depolymerization extents for the base case in **g** and **h** are 80%, 85%, 90% and 85% for PET, PLA, PBAT and PBS, respectively. Raw data for figures are provided in Supplementary Tables 13–20.

compositions and mechanical properties⁵². Accordingly, downstream processing steps must ultimately account for the wide variety of monomers present in other polyesters. In future work, the implications for downstream processing and monomer reclamation must be carefully

balanced and considered when expanding the accepted feedstocks in a mixed chemical recycling process.

Monomer purity is a critical parameter in chemical recycling processes. In a previous study, our group established tolerance windows

for monomer contamination during the synthesis of polyesters from waste-derived molecules⁵³. These findings informed the purity requirements for the present study, where a minimum monomer purity of 99% (as measured by DSC) was targeted⁵⁴. In part due to the rigorous monomer purity requirements in polycondensation reactions, product recovery from ACM represents the largest contribution to energy consumption in this chemical recycling technology (Fig. 5f). This presents an opportunity for future process improvement by replacing energy-intensive distillations for DMA–DMS or EG–BDO separation with lower energy alternatives such as counter-current extraction, simulated moving bed chromatography or reactive distillation. Here we demonstrated that such changes in the monomer reclamation process can have substantial impacts on energy consumption. Implementation of LLE to separate diester from diol monomers reduced the energy use of this process area by 68% compared with our previous study²⁹. Future work will include the investigation of lower-energy monomer recovery and the adoption of continuous processing to more closely mimic the process model.

Extents of depolymerization below 90% combined with monomer loss throughout the separation steps decreases process efficiency and raises product costs (Fig. 3b). The residual oligomeric fraction that is separated from the bottoms in DMT distillation could be recycled to increase overall yields. Optimization of the AC treatment process—through additional functionalization, porosity control, or recovery of monomers from the regenerated column effluent via LLE—could further enhance monomer recovery^{55–58}. Another strategy to reduce the cost of monomer reclamation is to lower the requirements for monomer purity in repolymerization. A study on the impact of minor but structurally similar monomer impurities, such as EG content in PBAT or DMA in PBS, and their impact on recycled polymer properties would be insightful for the design of future plastic materials and chemical recycling technologies.

TEA and LCA provide valuable guidance for directing process optimizations to have the largest impacts on product MSP and process emissions, respectively. For example, equipment required for polymerization contributes substantially to the capital investment required for building a commercial recycling plant (21%; Fig. 5a). In practice, this process step would ideally use or integrate with existing external polymerization facilities to decrease required capital investment. In some cases, polymer producers may need to hydrolyze the methyl ester monomers to be compatible with their polymerization facilities. The cost of monomer hydrolysis is expected to be less than that of polymerization²⁹. However, this would also change energy requirements, and thus the LCA results would need to be reevaluated. In addition, changing from traditional natural gas to RNG decreased process GHG emissions by 44%. The substantial decrease in energy use observed when implementing LLE for diol–diester separation demonstrates the impact of using process modeling to guide experimental optimization, and future efforts to improve this recycling process will continue to follow TEA and LCA direction.

Conclusion

Here we presented an efficient process for the chemical recycling of mixed polyester plastics. A design of experiments approach was utilized to optimize ACM conditions regardless of feedstock ratio, and WAXS indicated that changes in the polymer melt temperature correlated with reactivity under methanolysis conditions. The process was scaled to 1 kg of mixed feedstocks with high monomer yields. PET synthesized from DMT purified from the deconstruction of postconsumer waste showed no difference in mechanical or thermal properties compared with polymer made from commercial monomers. AC treatment was shown to be effective in removing dyes and metals from postconsumer plastic substrates, and implementation of an LLE step efficiently separated diol and diester monomers. TEA and LCA estimated that, at commercial scale, this process would reduce the MSP for the polyester

products by 36% while reducing GHG emissions by 41%. The reported technology is currently best suited for recycling mixed polyester packaging waste, such as multilayer food packaging that combines multiple polyesters or agricultural film waste (for example, PBAT–PLA blends) that are heavily soiled and difficult to recycle mechanically. However, the technology could expand into PET-rich textile recycling as well. Implementation of such a mixed polyester recycling technology, coupled with the increased use of bio-based plastics, could move us closer toward a net-zero circular plastics economy.

Methods

Materials

All reagents were used as received unless otherwise noted. The characterization of all polymers used in this study by thermogravimetric analysis, DSC, GPC and nuclear magnetic resonance can be found in Supplementary Information section I. Semi-crystalline PET powder was purchased from Goodfellow USA (lot #ES306031). PLA granules were received from NatureWorks as a research sample (Ingeo 4043D, lot #II1528B123). PBAT granules were received from BASF as a research sample (EcoFlex F Blend C1200, lot #54426956P0). PBS granules were received from Mitsubishi Chemical Corporation as a research sample (BioPBS, FZ91). Postconsumer PET bottle flake was received from Global Plastics Recycling as a research sample. Mater-Bi PLA/PBAT compatibilized film was purchased from <https://www.amazon.com/>. M&M's compostable PBS bags were purchased from Whole Foods.

DMT ($\geq 99\%$) was purchased from Sigma-Aldrich and recrystallized from 80 °C MeOH before use in polymerization. ML ($> 98\%$) was purchased from TCI America. DMA ($\geq 99\%$) was purchased from Sigma-Aldrich. DMS ($> 98\%$) was purchased from TCI America. Reagent-grade EG was purchased from VWR. BDO (99%), hexane ($\geq 99\%$), heptane (99%) and octane ($\geq 99\%$) were purchased from Aldrich. Methanol (electronic grade) was purchased from J.T. Baker. DMEA ($\geq 99\%$) was purchased from Sigma-Aldrich. Methylene chloride (DCM, HPLC grade, hydrocarbon stabilized) was purchased from Spectrum Chemical. Chloroform-*d*, (99.8% *D*) was purchased from Sigma-Aldrich. 1,1,1,3,3,3-Hexafluoroisopropanol (HFIP, $\geq 99\%$, HPLC grade) was purchased from Chem-Impex and filtered through a 0.1-μm polytetrafluoroethylene laminated filter before use. Sodium trifluoroacetate (NaTFAc, 98%) was purchased from Sigma-Aldrich. ICP-MS was performed by Intertek Pharmaceuticals. Procedures for all analytical methods can be found in Supplementary Information section XVI.

Polyester methanolysis in a sand bath

Sand bath methanolysis reactions were run in 14-ml Swagelok tube reactors. Details and part numbers, along with information about the fluidized sand bath reactors, can be found in Supplementary Information section II. For a reaction run under standard conditions, namely 20 wt% polymers in MeOH and 5 wt% DMEA, 2 g total polymer(s), 8.00 g MeOH (10.1 ml, 250 mmol) and 0.100 g DMEA (143 μl, 1.37 mmol), were added to a reactor. The reactor was sealed using anti-seize paste and tightened using a wrench and bench vise. The total mass of the reactor was recorded. Typically, 9–12 reactions were loaded and run in a single day, and all reactions were performed in triplicate. Each reactor was thoroughly shaken to mix the reagents before being heated. The reactors were then dropped into a basket immersed in the fluidized sand bath reactor preheated to the reaction temperature. Using this method, reactors with the longest residence time were added to the sand bath first, and reactors with the shortest residence time were added last. After the desired residence time, the entire basket was removed and quenched in an ice water bath for 20 min.

After quenching, the mass of each reactor was measured to ensure that it did not leak. The cap was then loosened using a wrench and bench vise. The reaction mixture was filtered using a 60-ml-capacity 10-μm-pore-size plastic filter (for which the mass was measured ahead of time), and the soluble fraction was collected directly into a 20-ml

vial (for which the mass was also measured ahead of time). The solids in the filter were washed with methanol to a total soluble fraction volume of 20 ml. Solids in the filter were dried in a vacuum oven at 50 °C overnight. In this way, the soluble monomeric products were isolated in the liquid fraction and any residual polymeric material along with DMT (if present) were isolated in the solid fraction.

Polyester methanolysis in a 300-ml pressure reactor

Methanolysis reactions run at the 200-ml scale were performed in a 300-ml Parker Autoclave Engineers EZE-Seal pressure vessel with overhead mechanical stirring. For a reaction run under ‘standard conditions’, namely 20 wt% polymers in MeOH and 10 wt% DMEA, 36 g total polymer(s), 144 g MeOH (180 ml, 4.49 mol) and 3.61 g DMEA (5.14 ml, 49.2 mmol) were added to the reactor vessel. The catalyst loading was increased slightly to account for volatile DMEA loss during reactor headspace purging. The vessel was then attached to the reactor, sealed using a torque wrench, and purged three times with nitrogen at 400 psi to remove oxygen from the reactor and prevent catalyst oxidation during the reaction. The reactor was sealed at ambient pressure, then heated to the desired temperature. Thirty minutes were added to the reaction time to account for the temperature ramp. The mechanical stirrer was run at ~600 rpm. After the reaction, the heating jacket was removed and the reactor vessel was quenched in an ice water bath for 30 min, any excess pressure was vented from the vessel, and it was removed from the reactor. The reaction mixture was filtered using a 100-ml-capacity 10-μm-pore-size plastic filter (for which the mass was measured ahead of time), and the soluble fraction was collected into a vacuum flask. The solids in the filter were washed with methanol to a total soluble fraction volume of 250 ml. Solids in the filter were then dried in a vacuum oven at 50 °C overnight.

Polyester methanolysis in a 7.7-liter pressure reactor

Methanolysis reactions run at the 5.5-liter scale were performed in a 7.7-liter movable head reactor from Parr with overhead mechanical stirring (Model #4552). For a reaction run under ‘standard conditions’, namely 20 wt% polymers in MeOH and 10 wt% DMEA, 1 kg total polymer(s), 3.80 kg MeOH (4.80 l, 119 mol), and 100 g DMEA (143 ml, 1.37 mol) were added to the reactor vessel. The catalyst loading was increased slightly to account for volatile DMEA loss during reactor headspace purging. The filled vessel was then sealed using a wrench and purged three times with nitrogen at 400 psi to remove oxygen from the reactor and prevent catalyst oxidation during the reaction. The reactor was sealed at ambient pressure, then heated to the desired temperature. Sixty minutes were added to the reaction time to account for the temperature ramp. The mechanical stirrer was run at ~600 rpm. After the reaction, the reactor vessel was quenched using a chilled water loop for 60 min, any excess pressure was vented from the vessel and it was removed from the reactor. The reaction mixture was filtered using a 2-liter-capacity Buchner funnel equipped with 11-μm-pore-size Whatman filter paper, and the soluble fraction was collected into a 4-liter vacuum flask. The solids in the filter were washed with methanol to a total soluble fraction volume of 6 liters. Solids in the filter were then dried in a vacuum oven at 50 °C overnight.

WAXS sample preparation

Borosilicate glass capillaries (1.4 mm inner diameter, 1.7 mm outer diameter and 100 mm length) were procured from AAdvance Instruments for the WAXS experiments. Before measurement, the capillaries were filled either solely with polymer or with a slurry of polymer, solvent and/or catalyst for one-quarter of their length, while the remaining two-quarters were filled with solvent and/or catalyst. After filling, the capillaries were flame-sealed for the measurements.

WAXS measurements

WAXS experiments were conducted at beamline 1–5 of the Stanford Synchrotron Radiation Lightsource at the SLAC National Accelerator

Laboratory, Menlo Park, USA. Beamline 1–5 was equipped with a pips diode to measure transmitted intensity and photon counting area detector Pilatus 100k (487 × 195 pixels, 172 × 172 μm² pixel size; Dectris AG) for WAXS measurement. The X-ray beam was microfocused with a spot size of approximately 500 × 500 μm² and an energy of 15 keV. The sample-to-detector distance was set to 1.53 m with a horizontal tilt angle of 29.1° and vertical tilt angle of −4.6° for WAXS detector. The sample-to-detector distance and horizontal and vertical tilt angles were calibrated using lanthanum hexaboride (LaB₆). The WAXS setup provided a resolvable spectrum of scattering vector (*q*-range) of 11–49 nm^{−1}.

In-situ heating stage coupled with WAXS setup

A custom-designed *in situ* heating stage, capable of accommodating up to three capillary sets, was used for the measurement. This heating stage allows for gradual temperature increases in the samples.

For the study of methanol effect on polymers, each polymer sample with and without methanol and their corresponding background, methanol and empty capillary, were measured, respectively at three spots separated by 1 mm (each spot for 30 s) in transmission mode. Temperature increases were carried out stepwise from room temperature to 200 °C with a 10 °C step. Frames acquired from each spot at the same temperatures were subsequently averaged in the final data analysis for each sample.

Furthermore, for the deconstruction measurement, a capillary filled with the reaction mixture (PET:PLA:PBAT in 50:25:25 ratio + methanol + DMEA) and another capillary containing methanol and DMEA as the background were positioned in two separate locations on the heating stage for the measurement. The temperature was continuously ramped from room temperature to 190 °C, then held at 190 °C for about 6 h before being cooled back to room temperature. During the deconstruction measurement, frames were acquired every 10 s. Three consecutive frames were averaged for data analysis, with the corresponding time durations also averaged for the resulting frame. The Python-based PyFai package⁵⁹ was used for data reduction and Python for data correction and analysis.

Reconstruction of PET from postconsumer materials

The deconstruction reaction was run in a 300-ml pressure reactor using a 90:9:1 ratio of postconsumer PET bottle flake to Mater-Bi PLA/PBAT compatibilized film to M&M’s compostable PBS bags. The methanolysis reaction was run under standard conditions (20 wt% polymers in MeOH and 10 wt% DMEA relative to polymers, 36 g total polymers) using the previously described procedure.

After drying in a vacuum oven, crude DMT (20.95 g) was purified for PET reconstruction by sequenced distillation and recrystallization. First, a distillation was conducted at 150 °C under 2 Torr vacuum to remove any high-boiling and inorganic contaminants (18.85 g, 90.0% recovery). Second, the DMT was crystallized from 80 °C methanol to remove remaining low boiling contaminants (15.25 g, 80.8% recovery). Wet DMT crystals were placed in a vacuum oven (40 °C) to dry overnight. Dried and purified DMT was then analyzed by elemental analysis, ICP-MS, GC-MS and DSC (Supplementary Information section VIII), indicating 99.4% purity.

Polycondensation was carried out in a glass reactor setup consisting of a 100-ml three-neck round-bottom flask (RBF) equipped with distillation/collection glass components, an IKA NANOSTAR 7.5 Digital mechanical stirring motor equipped with a steel stirring rod and paddle, an Ace Glassware 2 Torr diaphragm vacuum pump and a 2-liter-size Glas Col heating mantle equipped with a stainless-steel bowl inset filled with bismuth-tin low-melting (~138 °C) metal alloy (McMaster Carr). Heat was monitored by an in-house thermocouple unit in communication with the heating mantle.

PET synthesis consisted of charging the three-neck RBF with DMT (5.00 g, 0.02577 mol), EG (3 equivalent, 4.80 g) and titanium(IV)

isopropoxide catalyst (50 µl) all while under continuous flow of N₂. Polycondensation was performed in three steps. (1) The heat mantle was set to 180 °C under a constant stirring speed of 50 rpm and allowed to react overnight (~16 h), during which time the metal entered a molten state and the DMT was esterified to BHET, releasing methanol. (2) Once no further methanol collection was observed, the mantle was set to 250 °C for 1 h. (3) The mantle was then set to 280 °C for polycondensation over 6 h, and the atmosphere was gently switched from N₂ to vacuum by gradually turning a partitioning firestone valve over the course of the first 30 min, to help remove released EG product. After the 6-h polycondensation, the mantle was powered down and the RBF atmosphere was replaced with N₂ during the cooling stage. Polymer residue, highly adhered to the glass RBF, was removed by dissolving in 50 °C HFIP and precipitating in vigorously stirring, cold methanol. This procedure was performed both with recrystallized commercial DMT and with purified DMT obtained from the deconstruction of postconsumer materials.

Contamination removal via AC

The soluble fraction obtained from methanolysis was processed through a fixed-bed column packed with AC to eliminate dyes and trace metals. First, the AC packed column was prepared as follows. The granular AC particles (20–40 mesh) were soaked in ultrapure water and sonicated to remove air bubbles from the pore phase. After decanting the water, the AC (0.7 g) was redissolved in fresh ultrapure water to prepare about 50 v/v% AC slurry. The slurry was loaded onto an Omnifit column (1 cm inner diameter and 10 cm height) and packed down by flushing with water at 10 ml min⁻¹ for 30 min. After the slurry was packed down, the column length was finally adjusted to 5 cm height with a plunger.

The AC column was connected to a Buchi Pure flash chromatography system (C-815), equipped with a radial piston pump, an evaporative light scattering detector (ELSD), and an ultraviolet (UV)–visible (200, 230, 250, and 280 nm) spectrophotometer. The AC column was saturated with methanol (2 ml min⁻¹) to achieve baseline ELSD and UV–visible signals before and after loading the monomer mixtures. The methanolysis reaction mixture after filtration was directly loaded onto the AC column at 2 ml min⁻¹. After a breakthrough curve reached a plateau, methanol was loaded to wash the AC column until the UV signal returned to the baseline. Effluent fractions were collected every 2 ml for monomer and trace metal analysis by GC–MS and ICP–MS, respectively.

LLE for diol and ester separation

The separation of mixed diols (BDO and EG) and esters (DMA and DMS) was achieved through LLE in batch mode. Three LLE solvent systems were tested, including (1) pentane, (2) hexane and (3) heptane. The monomer mixture was mixed with varying volumes of these solvents (volume ratios of 1, 2, 4, 8 and 16) in a separatory funnel. After thorough mixing, the upper (organic phase) and lower (aqueous phase) layers were formed after about 10 min and the two phases were separated.

The monomer mixture volume was 4 ml, with the volume ratio of BDO, EG, DMA and DMS being 1:1:1:1. The volume of each solvent system was calculated according to the volume ratios of 1, 2, 4, 8 and 16. The solvent volume was calculated by multiplying the volume of the monomer mixture (4 ml) by the volume ratio factor.

Two approaches were used for the separation systems: a single-step LLE and a two-step LLE. The single-step procedure involved mixing the monomer mixture with the solvent once, followed by phase separation. The two-step process started with mixing half the total volume of solvent with the monomer mixture, separating the upper phase, then mixing the remaining solvent with the aqueous phase and finally separating the phases again.

Inclusion and ethics

One or more of the authors of this paper self-identifies as a member of the LGBTQ+ community. One or more of the authors of this paper self-identifies as an underrepresented ethnic minority in science. While

citing references scientifically relevant to this work, we also actively worked to promote gender balance in our reference list.

Data availability

The data that supports the findings presented in this Article are available in the Supplementary Information.

References

1. Spierling, S. et al. Bio-based plastics—a review of environmental, social and economic impact assessments. *J. Clean. Prod.* **185**, 476–491 (2018).
2. Zheng, J. & Suh, S. Strategies to reduce the global carbon footprint of plastics. *Nat. Clim. Change* **9**, 374–378 (2019).
3. Meys, R. et al. Achieving net-zero greenhouse gas emission plastics by a circular carbon economy. *Science* **374**, 71–76 (2021).
4. Gabisa, E. W., Ratanatamskul, C. & Gheewala, S. H. Recycling of plastics as a strategy to reduce life cycle GHG emission, microplastics and resource depletion. *Sustainability* **15**, 15 (2023).
5. Tenhunen-Lunkka, A., Rommens, T., Vanderreydt, I. & Mortensen, L. Greenhouse gas emission reduction potential of European Union's circularity related targets for plastics. *Circ. Econ. Sustain.* **3**, 475–510 (2023).
6. Vidal, F. et al. Designing a circular carbon and plastics economy for a sustainable future. *Nature* **626**, 45–57 (2024).
7. Zia, K. M., Noreen, A., Zuber, M., Tabasum, S. & Mujahid, M. Recent developments and future prospects on bio-based polyesters derived from renewable resources: a review. *Int. J. Biol. Macromol.* **82**, 1028–1040 (2016).
8. Feghali, E., Tauk, L., Ortiz, P., Vanbroekhoven, K. & Eevers, W. Catalytic chemical recycling of biodegradable polyesters. *Polym. Degrad. Stab.* **179**, 109241 (2020).
9. Filiciotto, L. & Rothenberg, G. Biodegradable plastics: standards, policies, and impacts. *ChemSusChem* **14**, 56–72 (2021).
10. Payne, J. & Jones, M. D. The chemical recycling of polyesters for a circular plastics economy: challenges and emerging opportunities. *ChemSusChem* **14**, 4041–4070 (2021).
11. Zhang, Q. et al. Bio-based polyesters: recent progress and future prospects. *Prog. Polym. Sci.* **120**, 101430 (2021).
12. Hackett, M., Zeng, L. & Masuda, T. *Biodegradable Polymers* (IHS Markit, 2021).
13. Clark, R. A. & Shaver, M. P. Depolymerization within a circular plastics system. *Chem. Rev.* **124**, 2617–2650 (2024).
14. Shi, C., Quinn, E. C., Diment, W. T. & Chen, E. Y. X. Recyclable and (bio)degradable polyesters in a circular plastics economy. *Chem. Rev.* **124**, 4393–4478 (2024).
15. Coates, G. W. & Getzler, Y. D. Y. L. Chemical recycling to monomer for an ideal, circular polymer economy. *Nat. Rev. Mater.* **5**, 501–516 (2020).
16. Ellis, L. D. et al. Chemical and biological catalysis for plastics recycling and upcycling. *Nat. Catal.* **4**, 539–556 (2021).
17. Li, H. et al. Expanding plastics recycling technologies: chemical aspects, technology status and challenges. *Green Chem.* **24**, 8899–9002 (2022).
18. Yang, R., Xu, G., Dong, B., Guo, X. & Wang, Q. Selective, sequential, and “one-pot” depolymerization strategies for chemical recycling of commercial plastics and mixed plastics. *ACS Sustain. Chem. Eng.* **10**, 9860–9871 (2022).
19. Spicer, A. J., Brandoles, A. & Dove, A. P. Selective and sequential catalytic chemical depolymerization and upcycling of mixed plastics. *ACS Macro Lett.* **13**, 189–194 (2024).
20. Zhang, Q. et al. Solvent-promoted catalyst-free recycling of waste polyester and polycarbonate materials. *ACS Macro Lett.* **13**, 151–157 (2024).

21. Allen, R. D. & James, M. I. in *Circular Economy of Polymers: Topics in Recycling Technologies* Vol. 1391 Ch. 4 (American Chemical Society, 2021).
22. *Bioplastics Market Development Update 2023* (European Bioplastics, 2023).
23. van Oers, L., van der Voet, E. & Grundmann, V. in *Global Risk-Based Management of Chemical Additives I: Production, Usage and Environmental Occurrence* (eds Bilitewski, B., Darbra, R. M., & Barceló, D.) 133–149 (Springer, 2012).
24. Hahladakis, J. N., Velis, C. A., Weber, R., Iacovidou, E. & Purnell, P. An overview of chemical additives present in plastics: migration, release, fate and environmental impact during their use, disposal and recycling. *J. Hazard. Mater.* **344**, 179–199 (2018).
25. Horodytska, O., Cabanes, A. & Fullana, A. Non-intentionally added substances (NIAS) in recycled plastics. *Chemosphere* **251**, 126373 (2020).
26. Turner, A. & Filella, M. Hazardous metal additives in plastics and their environmental impacts. *Environ. Int.* **156**, 106622 (2021).
27. Nicholson, S. R. et al. The critical role of process analysis in chemical recycling and upcycling of waste plastics. *Annu. Rev. Chem. Biomol. Eng.* **13**, 301–324 (2022).
28. Nixon, K. D. et al. Analyses of circular solutions for advanced plastics waste recycling. *Nat. Chem. Eng.* **1**, 615–626 (2024).
29. DesVeaux, J. S. et al. Mixed polyester recycling can enable a circular plastic economy with environmental benefits. *One Earth* **7**, 2204–2222 (2024).
30. Gruber, P. R. et al. Continuous process for the manufacture of a purified lactide from esters of lactic acid. US5247059A (1993).
31. Kulkarni, R. V. & Dominguez, L. Production of polyester using preblended cobalt–phosphorus. US6793083B2 (2004).
32. Witt, U. & Yamamoto, M. Method for the continuous production of biodegradable polyesters. US8614280B2 (2015).
33. Cuthbertson, A. A. et al. Characterization of polymer properties and identification of additives in commercially available research plastics. *Green Chem.* **26**, 7067–7090 (2024).
34. Chen, J. Y., Ou, C. F., Hu, Y. C. & Lin, C. C. Depolymerization of poly(ethylene terephthalate) resin under pressure. *J. Appl. Polym. Sci.* **42**, 1501–1507 (1991).
35. Jaime-Azuara, A., Longo, E., Boselli, E., Baratieri, M. & Pedersen, T. H. Exploratory DSC investigation on the solvolytic depolymerization of PET in varied solvent systems and in the presence of model additives and contaminants. *Polym. Degrad. Stab.* **224**, 110751 (2024).
36. Huggins, M. L. Solutions of long chain compounds. *J. Chem. Phys.* **9**, 440–440 (1941).
37. Flory, P. J. Thermodynamics of high polymer solutions. *J. Chem. Phys.* **10**, 51–61 (1942).
38. Kim, M.-H. & Glinka, C. J. Application of in situ vapor sorption small-angle neutron scattering (SANS) to semicrystalline polymers: vapor pathway and structure evolution in semicrystalline linear polyethylene. *J. Appl. Crystallogr.* **38**, 734–739 (2005).
39. Murthy, N. S., Akkapeddi, M. K. & Orts, W. J. Analysis of lamellar structure in semicrystalline polymers by studying the absorption of water and ethylene glycol in nylons using small-angle neutron scattering. *Macromolecules* **31**, 142–152 (1998).
40. Scheirs, J. *Polymer Recycling: Science, Technology and Applications* (Wiley, 1998).
41. Model bale specifications. Association of Plastic Recyclers <https://plasticsrecycling.org/model-bale-specifications> (2022).
42. Filella, M. Antimony and PET bottles: checking facts. *Chemosphere* **261**, 127732 (2020).
43. Kamimura, A., Akinari, Y., Watanabe, T., Yamada, K. & Tomonaga, F. Efficient chemical recycling of waste fiber-reinforced plastics: use of reduced amounts of dimethylaminopyridine and activated charcoal for the purification of recovered monomer. *J. Mater. Cycles Waste Manag.* **12**, 93–97 (2010).
44. Huang, J. et al. Removal of trace amount impurities in glycolytic monomer of polyethylene terephthalate by recrystallization. *J. Environ. Chem. Eng.* **9**, 106277 (2021).
45. Cooney, D. O., Nagerl, A. & Hines, A. L. Solvent regeneration of activated carbon. *Water Res.* **17**, 403–410 (1983).
46. Jareteg, A., Maggiolo, D., Thunman, H., Sasic, S. & Ström, H. Investigation of steam regeneration strategies for industrial-scale temperature-swing adsorption of benzene on activated carbon. *Chem. Eng. Process. Process Intens.* **167**, 108546 (2021).
47. Parodi, A., Arpaia, V., Samori, C., Mazzocchetti, L. & Galletti, P. Novel strategies for recycling poly(butylene adipate-co-terephthalate)-starch-based plastics: selective solubilization and depolymerization-repolymerization processes. *ACS Sustain. Chem. Eng.* **11**, 14518–14527 (2023).
48. Yang, X. et al. Biodegradable polyester mixture. US10526461B2 (2020).
49. Uekert, T., Walzberg, J., Wikoff, H. M., Doyle, M. M. & Carpenter, A. C. Strategies for considering environmental justice in the early-stage development of circular economy technologies. *ACS Sustain. Chem. Eng.* **12**, 8307–8312 (2024).
50. *Methanol Safe Handling Manual: 5th Edition* (The Methanol Institute, 2020).
51. EPA chemical list basic search. US Environmental Protection Agency https://guideme.epa.gov/ords/guideme_ext/f?p=guideme:chemical-list-basic-search (2024).
52. Clarke, R. W. et al. Polyhydroxyalkanoates in emerging recycling technologies for a circular materials economy. *Mater. Adv.* **5**, 6690–6701 (2024).
53. Clarke, R. W. et al. Re-directing mixed-feed deconstruction products to hybrid polyesters: tolerance windows for commodity plastics reconstruction. *Resour. Conserv. Recycl.* **222**, 108439 (2025).
54. Ho, J. et al. *Regional Energy Deployment System (ReEDS) Model Documentation (Version 2020)* (2021).
55. Bhatnagar, A., Hogland, W., Marques, M. & Sillanpää, M. An overview of the modification methods of activated carbon for its water treatment applications. *Chem. Eng. J.* **219**, 499–511 (2013).
56. Yu, C. et al. Adsorption removal of thiophene and dibenzothiophene from oils with activated carbon as adsorbent: effect of surface chemistry. *J. Porous Mater.* **15**, 151–157 (2008).
57. Zieliński, B., Miądlicki, P. & Przepiórski, J. Development of activated carbon for removal of pesticides from water: case study. *Sci. Rep.* **12**, 20869 (2022).
58. Li, M., Lu, J., Li, X., Ge, M. & Li, Y. Removal of disperse dye from alcoholysis products of waste PET fabrics by nitric acid-modified activated carbon as an adsorbent: kinetic and thermodynamic studies. *Text. Res. J.* **90**, 2058–2069 (2020).
59. Ashiotis, G. et al. The fast azimuthal integration Python library: pyFAI. *J. Appl. Crystallogr.* **48**, 510–519 (2015).

Acknowledgements

This work was authored in part by the National Renewable Energy Laboratory, operated by Alliance for Sustainable Energy, for the US Department of Energy (DOE) under contract number DE-AC36-08GO28308. Funding was provided by Amazon and the US DOE, Office of Energy Efficiency and Renewable Energy, Advanced Materials and Manufacturing Office and Bioenergy Technologies Office. This work was performed as part of the Bio-Optimized Technologies to keep Thermoplastics out of Landfills and the Environment (BOTTLE) Consortium. The views expressed in the Article do not necessarily represent the views of the DOE or the US

Government. The US Government retains a nonexclusive, paid-up, irrevocable, worldwide license to publish or reproduce the published form of this work, or allow others to do so, for US Government purposes. We thank E. Stone for preparing the table of contents figure, T. Uekert for contributing to the environmental risk assessment and for a detailed reading of the paper, C. Paepel for performing elemental analysis, C. Lincoln for performing GPC and J. Shane for providing postconsumer polyester substrates.

Author contributions

G.T.B., A.J.J. and K.M.K. contributed to the initial conceptualization. J.B.C. performed and analyzed the deconstruction experiments. J.B.C., A.K.M., S.A.H., Y.W. and C.J.T. planned, executed and analyzed the X-ray scattering experiments. Y.L. and H.C. performed and analyzed the monomer separation experiments. R.W.C. performed and analyzed the reconstruction experiments. J.S.D. developed the process and economic models and conducted the environmental analysis. J.B.C., Y.L., J.S.D., H.C., W.E.M., L.M.S., A.L.B., H.A.N., A.J.J., O.D.M. and K.M.K. contributed to the process design and analysis. J.B.C., J.S.D. and K.M.K. wrote the paper with contributions from all authors.

Competing interests

J.B.C., Y.L., J.S.D., H.C., O.D.M., G.T.B., A.J.J. and K.M.K. have submitted patent applications on the amine-catalyzed methanolysis of mixed polyesters and downstream monomer recovery. The corresponding patent application numbers are WO2024173754A1 and PCT/US24/37401, respectively. J.B.C. is the founder and CEO of EsterCycle. G.T.B. is an advisor to Samsara Eco and Tereform. K.M.K. is an advisor to EsterCycle and Tereform. The other authors declare no competing interests.

Additional information

Supplementary information Extended data is available for this paper at <https://doi.org/10.1038/s44286-025-00275-x>.

Supplementary information The online version contains supplementary material available at <https://doi.org/10.1038/s44286-025-00275-x>.

Correspondence and requests for materials should be addressed to Katrina M. Knauer.

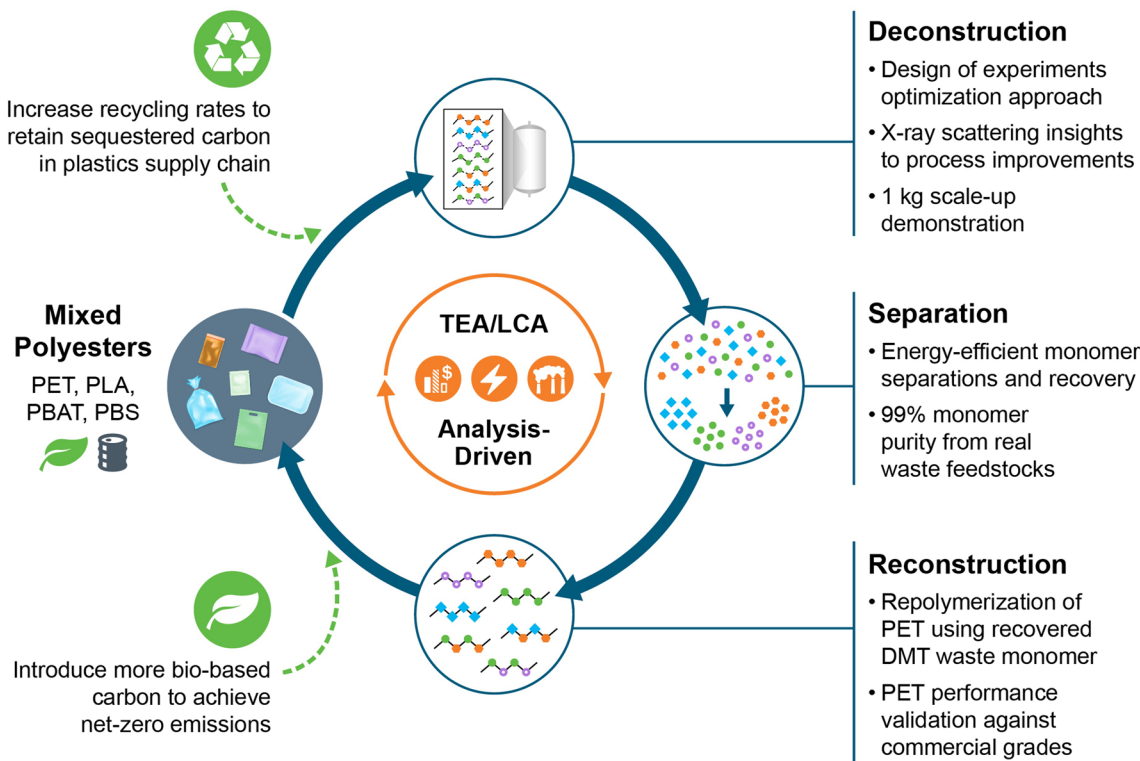
Peer review information *Nature Chemical Engineering* thanks Kevin M. Van Geem, Fan Zhang and the other, anonymous, reviewer(s) for their contribution to the peer review of this work.

Reprints and permissions information is available at www.nature.com/reprints.

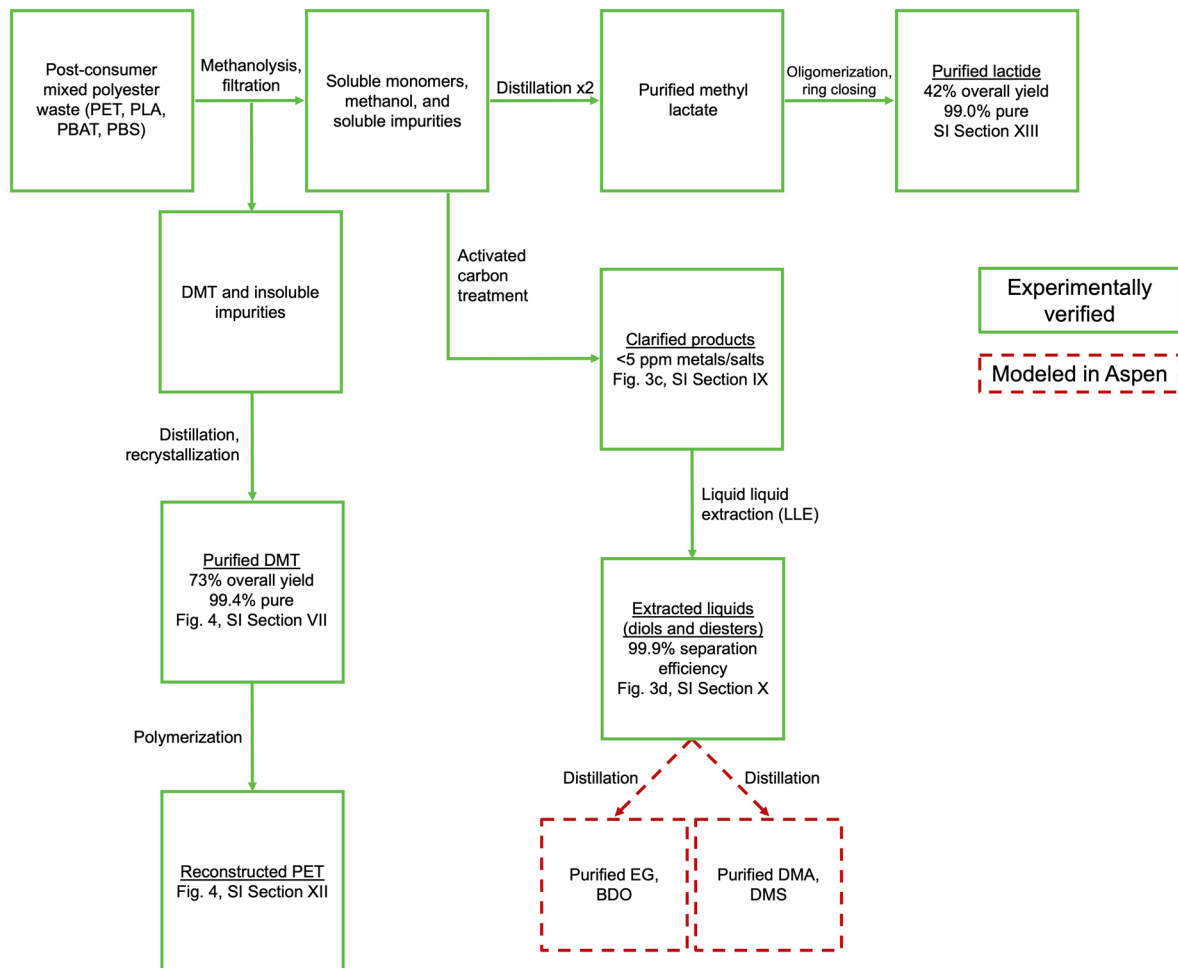
Publisher's note Springer Nature remains neutral with regard to jurisdictional claims in published maps and institutional affiliations.

Springer Nature or its licensor (e.g. a society or other partner) holds exclusive rights to this article under a publishing agreement with the author(s) or other rightsholder(s); author self-archiving of the accepted manuscript version of this article is solely governed by the terms of such publishing agreement and applicable law.

© The Author(s), under exclusive licence to Springer Nature America, Inc. 2025



Extended Data Fig. 1 | Circular polyester chemical recycling. Overview of the analysis-driven circular methanolysis process reported here and its primary steps.



Extended Data Fig. 2 | Detailed process flow diagram for monomer separations. Individual sub-processes are shown as labeled. Monomer purity was determined via DSC. Metal content was determined via ICP-MS. Separations/purification steps highlighted in solid green were experimentally validated and steps highlighted in dashed red were modeled in Aspen.